Long-term stability of ferri-/ferrocyanide as an electroactive component for redox flow battery applications: On the origin of apparent capacity fade

Eric M. Fell[1], Diana De Porcellinis[1], Yan Jing[2], Valeria Gutierrez-Venegas[3], Roy G. Gordon[2], Sergio Granados-Focil[3], Michael J. Aziz[1,z,]

[1] Harvard John A. Paulson School of Engineering and Applied Sciences, 29 Oxford Street, Cambridge, MA, 02138, USA.
[2] Department of Chemistry and Chemical Biology, Harvard University, 12 Oxford Street, Cambridge, MA, 02138, USA.
[3] Gustaf Carlson School of Chemistry and Biochemistry, Clark University, Worcester, MA, 01610-1477, USA.
[z]corresponding author, maziz@harvard.edu

Abstract

We assess the suitability of potassium ferri-/ferrocyanide as an electroactive species for long-term utilization in aqueous organic redox flow batteries. A series of electrochemical and chemical characterization experiments was performed to distinguish between structural decomposition and apparent capacity fade of ferri-/ferrocyanide solutions used in the capacity-limiting side of a flow battery. Our results indicate that, in contrast with previous reports, no structural decomposition of ferri-/ferrocyanide occurs at tested pH values as high as 14 in the dark or in diffuse indoor light. Instead, an apparent capacity fade takes place due to an electroless reduction of ferricyanide to ferrocyanide, via electroless oxygen evolution reaction. We find that this parasitic process can be further exacerbated by carbon electrodes, with apparent capacity fade rates at pH 14 increasing with an increased ratio of carbon electrode surface area to total amount of ferricyanide in solution. Based on these results, we report a set of operating conditions that enables the cycling of alkaline ferri-/ferrocyanide electrolytes, and demonstrate how apparent capacity fade rates can be engineered by the initial cell setup. If protected from direct exposure to light, the chemical stability of ferri-/ferrocyanide anions allows for their practical deployment as electroactive species in long duration energy storage applications.

Introduction

As the global demand for sustainable electric power generation increases, aqueous organic redox flow batteries (AORFBs) offer a potential solution to the intermittency of solar and wind resources. The non-flammable electrolytes used in AORFBs contain redox-active species synthesized from earth-abundant elements. Following the initial introduction of redox-active organics in the negolyte (negative electrolyte) of an aqueous flow battery [1], many promising redox-active molecules have been developed as candidates for acidic, alkaline, and neutral environments [2-17]. In contrast, very few redox-active molecules have been demonstrated as promising species for the posolyte (positive electrolyte) [3,18-25]. Long-term stability of redox-active molecules [13], or the ability to recompose degraded molecules [11,26], is a critical feature required for practical utility in a battery.

The best candidate for the posolyte in an alkaline environment continues to be ferri-/ferrocyanide, $Fe(CN)_6^{3-}$/ $Fe(CN)_6^{4-}$. The ferri-/ferrocyanide anion has been studied since 1839 [27]. It has long been known that exposing neutral or alkaline pH solutions of ferrocyanide to light of wavelengths less than ~500 nm leads to chemical degradation of the anion to pentacyanide/iron hydroxides, whereas aqueous solutions of ferrocyanide kept in the dark, or in diffuse indoor light, are chemically stable [28-30]. In acidic conditions, ferri-/ferrocyanide is well known to release free cyanide into solutions, generating hydrogen cyanide (HCN). In early work on zinc–ferrocyanide RFBs, Adams *et al*. saw that ferri-/ferrocyanide is chemically stable in up to 7N NaOH at temperatures as high as 50°C, but above that, ferricyanide began to decompose into electrochemically inactive pentacyanide, and further insoluble iron hydroxides [18]. They also hypothesized that a very slow chemical degradation of ferricyanide due to cyanide loss may occur, however, they noted that their starting material contained pentacyanide impurities, thus calling in to question whether any observed cyanide ligand loss was due to a spontaneous process, or decomposition promoted by the already present pentacyanides. Their work also noted that pentacyanides in solution can be rejuvenated back to ferrocyanide by the addition of free cyanide. However, it is only recently that this coordination compound has been reported to appear extremely unstable in dark, alkaline, conditions at room temperature. A study by Luo *et al.* observed rapid capacity fade while cycling alkaline ferri-/ferrocyanide electrolytes in a capacity-balanced symmetric cell flow battery at high pH [31]. The researchers attributed the decrease in capacity to chemical decomposition of ferri-/ferrocyanide via cyanide ligand dissociation from the iron center, and subsequent irreversible hydroxylation of the coordination compound. Soon after, Goulet and Aziz [32] reported the reduction of ferricyanide to ferrocyanide occurring when in contact with carbon paper electrodes, noting that the reaction rate appeared pH-dependent. More importantly, they did not observe irreversible chemical decomposition of ferri-/ferrocyanide in *ex situ* characterization of cycled electrolytes, calling into question the results of [31]. Cazot *et al.* [33] observed significantly lower capacity fade rates in ferri-/ferrocyanide symmetric cells at high pH and noted that fluctuating membrane resistance during cell cycling could partially explain the apparent fade demonstrated in ref. [31] due to the use of purely galvanostatic cycling. Páez *et al*. [34] revisited the experiments performed in ref. [31] and further disproved the claims of ferri-/ferrocyanide chemical instability in alkaline conditions. They also proposed that cell unbalancing due to the electrochemical oxygen evolution reaction (OER) could play an important role in the observed apparent cycling capacity fade, as previously hypothesized in [32]. Most recently, in a follow up to their previous work of ref. [31], the Liu group once again reported findings [35] of ferri-/ferrocyanide cyanide ligand dissociation and subsequent irreversible hydroxylation but could demonstrate this degradation mechanism only under conditions of artificial addition of free cyanide in solution, and of light illumination. Once again, rapid apparent capacity fade was attributed to an irreversible chemical degradation, but *ex situ* ^{13}C NMR and UV-Vis data were inconsistent with the apparent extreme loss of capacity. They further propose that the previously observed parasitic reduction of ferricyanide to ferrocyanide in alkaline conditions is balanced by a chemical oxidation of the proposed dissociated cyanide (CN^-) to cyanate (OCN^-). However, the validity of this mechanism hinges on the requirement for ample free cyanide to be present in solution and, if correct, the mechanism requires a more nuanced interpretation involving hydroxide to both fully balance the hypothesized electroless reaction and explain observed pH-dependence. Thus, the proposed mechanism of ref. [35] would be applicable to a flow battery utilizing ferri-/ferrocyanide electrolytes only if free cyanide is present in solution. Herein, we explain the results of refs. [31] & [35] through a different mechanistic interpretation. Given that the instability of alkaline ferri-/ferrocyanide solutions in the presence of light has never been in question, it is the determination of chemical stability in the dark that is most pertinent to a lifetime evaluation of the use of ferri-/ferrocyanide electrolytes in commercial flow batteries.

Unfortunately, many of these studies have not followed what we have argued [8,13,32] to be the most robust setup and use of the symmetric cell, and the ways in which it can tease out capacity fade mechanisms. Although a powerful technique, a symmetric cell can measure the attainable capacity in each cycle only within the capacity limits of its initial reservoirs, where the accessible state-of-charge (SOC) range is determined by the initial reservoir configurations. Irreversible degradation of the redox-active species obviously decreases the measured capacity, but so does any shift in the accessible SOC. A parasitic reduction/oxidation of the redox-active species can result in a shift of accessible SOC, yet may appear coulometrically as an apparent capacity fade, thereby masking the real process that is occurring [32]. When used to determine molecular reactant stability, the requirements for a correct implementation of a symmetric cell include: i) the use of potentiostatic cycling, or galvanostatic with potential holds, to fully access the available capacity irrespective of possible drift or fluctuations in cell polarization resistance; ii) initiating the cell with volumetrically unbalanced compositionally-symmetric positive and negative electrolyte reservoirs (i.e. both start at 50% SOC, resulting in a well-defined initial 0 V open circuit voltage) so that a capacity limiting side is clearly identified and capacity fade solely in this reservoir can be investigated; iii) cycling cells in an inert atmosphere and light-controlled environment to prevent further confusion from electrolyte interactions with reactive gaseous species and photo-induced (electro)chemical reactions; and iv) reporting capacity fade rates as time-denominated rather than (or in addition to) cycle-denominated, which is more representative of the temporal dependence of chemical decay kinetics [32]. Symmetric cell methods implemented in refs. [31,34,35] are vulnerable to drift or fluctuations in cell resistance, and risk being thrown out of balance by side reactions, thereby restricting the accessible SOC range even in the absence of any active species loss. Thus, conflicting reports still exist within the AORFB community concerning the cycling stability of alkaline ferri-/ferrocyanide electrolytes, and how best to reproducibly evaluate said stability through cell cycling procedures.

We have re-examined the chemical stability, in the dark, of ferri-/ferrocyanide in alkaline conditions using a series of experiments designed to unambiguously determine whether the measured capacity fade arises from irreversible chemical degradation or reversible chemical or electrochemical side reactions. Electrochemical and chemical stability have been analyzed for both pristine electrolytes and electrolytes subjected to electrochemical cycling in flow cells. Coulometric analysis was first performed utilizing the volumetrically unbalanced, compositionally symmetric cell technique[32]. The *ex situ* methods of NMR and UV-Vis absorption spectrophotometry were employed to distinguish between real (electrochemically irreversible) and apparent (electrochemically reversible) capacity fade. Our findings indicate that ferri-/ferrocyanide remains chemically stable in the dark in the tested range of pH 7-14, but that ferricyanide undergoes an electroless, parasitic reduction to ferrocyanide in alkaline conditions, facilitated by electroless OER acting as the balancing oxidation half-reaction. Notably, we find that the rate of the electroless reaction can be exacerbated when an alkaline solution containing ferricyanide is in contact with porous carbon electrodes, without any applied potential. We also demonstrate that the electrochemical cycling of alkaline ferri-/ferrocyanide electrolytes can be accomplished without promoting oxygen evolution from electrochemical splitting of water, suggesting that previous work [34] attributing capacity fade to the electrochemical OER, thus shifting the accessible SOC range and leading to cell unbalancing, requires a different interpretation. Our work suggests that cyanide ligand dissociation of ferri-/ferrocyanide is a photocatalytic process, rather than a mechanism occurring independent of light exposure as previously proposed in refs. [31] & [35]. We also describe how the rate of apparent capacity fade in ferri-/ferrocyanide symmetric cells depends on pH and the ratio of total ferricyanide to carbon electrode surface area, defined by the initial configuration of electrolyte reservoirs in a given cell. Based on these results, we have determined a set of conditions enabling the successful implementation of ferri-/ferrocyanide electrolytes in long duration energy storage applications. Furthermore, we demonstrate why an electroless reduction process in an electrolyte used extensively by the AORFB community typically avoids detection in standard full cell battery cycling. Our results provide insights into several approaches that may introduce artifacts that obscure the parasitic reduction process. Collectively, this work seeks to prevent the AORFB community from being misled into rejecting ferri-/ferrocyanide as a competitive posolyte species in alkaline conditions due to lifetime issues.

Experimental

Electrolyte preparation

Reagents used to prepare electroactive (posolyte and negolyte) solutions were purchased from Sigma Aldrich and used with no further purification: potassium hydroxide, potassium ferrocyanide trihydrate (99.5% purity), and potassium ferricyanide (99.5% purity). Throughout the manuscript we will be referring to these chemicals as KOH, ferrocyanide, and ferricyanide, respectively. Because atmospheric CO_2 readily dissolves into high pH solutions, we prevented carbonate formation by storing and cycling our solutions in an oxygen/CO_2-free glovebox (O_2 partial pressure less than 2 ppm). Electrolyte solutions used in cell cycling were also prepared inside the glovebox with degassed deionized water.

Electrode materials

Two different commercial electrodes were used: Sigracet GDL 39AA (Fuel Cell Store), and AvCarb HCBA 1186 carbon cloth (AvCarb Materials Solutions). Hereafter we refer to these electrodes as SGL and HCBA, respectively. SGL has an uncompressed thickness of 280 μm and HCBA has an uncompressed thickness of 1.3 mm. All electrodes were baked at 400°C in air for 24 h prior to use.

Cell assembly

Flow battery experiments were carried out with cell hardware from Fuel Cell Technologies Inc. (Albuquerque, NM), assembled into a zero-gap flow cell configuration, as described in a previous report [2]. Pyrosealed POCO graphite flow plates (9 in^2) with interdigitated flow patterns were used for both electrodes. Unless otherwise stated, each electrode comprised a 5 cm^2 geometric surface area covered by either a stack of two sheets of SGL, or one HCBA electrode, per side. The outer portion of the space between the electrodes was gasketed using Viton sheets (10 mils for SGL cells, 30 mils for HCBA cells) with the area over the electrodes cut out. The torque applied during cell assembly was 60 lb-in (6.78 N·m) on each of eight 3/8”–24 bolts, thus the load applied per bolt is approximately 800 lbs. Electrolytes were fed into the cell through fluorinated ethylene propylene (FEP) tubing at a rate of 60 mL/min, controlled by Cole-Parmer 6 Masterflex L/S peristaltic pumps. For all symmetric cell tests, a sheet of Nafion 117 (Ion Power Inc.) membrane served as the ion-selective membrane between the carbon electrodes. All membranes were presoaked in 1 M KOH for 3 days to ion exchange the counter ions from protons to potassium ions. If a membrane was to be tested in an electrolyte solution with a pH lower than 14, the membrane was then soaked for an additional day in a KOH solution with the target pH.

Cell cycling protocol

Cycling stability of the ferri-/ferrocyanide electrolyte was studied by the volumetrically unbalanced, compositionally symmetric cell method, as described elsewhere [32], hereafter referred to as a symmetric cell. Unless otherwise stated, the capacity-limiting side (CLS) and non-capacity limiting side (NCLS) contained identical starting solution compositions, both initially at 50% SOC i.e., equal concentrations of ferricyanide and ferrocyanide. Charge/discharge cell cycling was performed using a Biologic VSP-300 potentiostat. Each cell was potentiostatically charged/discharged at ±200 mV, with ±2 mA/cm^2 (geometric area) current cutoffs. The first cycle was always a charge cycle with respect to the CLS. All cells were run inside a glove box with minimal exposure to lab light.

^{13}C NMR

^{13}C NMR spectra were acquired from electrolyte solution aliquots taken before and after cycling. All samples were reduced to 100% ferrocyanide (Fe^{2+}) to avoid the signal interference from the paramagnetic ferricyanide (Fe^{3+}). For each sample, a 100 μL aliquot was taken from the starting solution of 0.1 M at pH 14 and diluted by adding 550 μL of D_2O in the glovebox. To avoid chemical shift inconsistencies caused by sample preparation and different pH, an internal standard of 20 μM dimethyl sulfoxide (DMSO) was added to the samples. All ^{13}C NMR samples were scanned 1000 times at room temperature to collect final spectra in an Agilent 500 MHz NMR instrument.

UV-Vis spectrophotometry

To confirm the chemical stability of ferricyanide, a 0.5 mM solution of ferricyanide in 1 M KOH was prepared and fractioned into small vials of 3 mL. As reported in a previous publication [32], the total iron concentration was measured with UV-Vis spectrophotometry (Varian, Cary 60) at a wavelength of 278 nm and the ferricyanide concentration at a wavelength of 420 nm. Since numerous studies have demonstrated that ferri-/ferrocyanide is susceptible to photocatalyzed decomposition [28-30] all the experiments were performed protecting the solutions from light by wrapping the vials with aluminum foil and keeping them stored in a closed box in a lab with no windows. To study the effect of the carbon electrode interaction, the same starting solution was added to several vials (3 mL) containing pieces (4 mm × 4 mm) of SGL or HCBA electrodes.

Results

Effect of pH on ferri-/ferrocyanide cycling stability

We first characterized the effect of pH on the observed capacity fade in symmetric cells by comparing four identical cell builds using SGL as electrodes, with 0.1 M ferri-/0.1 M ferrocyanide electrolytes at varying pH. As seen in Fig. 1, an exponential drop in capacity is observed when cycling ferri-/ferrocyanide symmetric cell flow batteries at highly alkaline pH. Given that capacity in AORFBs has typically been shown [32] to decrease exponentially over time – a behavior consistent with unimolecular decomposition kinetics – we report instantaneous temporal fade rates derived from the slope of the natural log of discharge cycle capacity vs time plot ($-d \ln C / dt$, where $C(t)$ is the time-dependent capacity). The plotted discharge capacities in Fig. 1a represent 118, 123, 155, and 103 cycles for pH 7, 12, 13, and 14, respectively. We do not report AORFB capacity fade rates in units of % per cycle as it is a meaningless figure of merit for time-denominated fade mechanisms when the cycle period changes due to a) ohmic resistance changes, and b) (apparent) capacity fade. Furthermore, comparing fade rates of cells that differ in initial capacity are futile if using % per cycle, unless the cycle period is identical between each cell. An increased rate of capacity fade with increase in pH can clearly be seen in Fig. 1, similar to the reported trend in [31]. However, a distinct difference in total capacity utilization must first be noted between our work and previous work demonstrating cell cycling of AORFB electrolytes. Each symmetric cell in Fig. 1 initially accesses >99% of the theoretical capacity of the CLS electrolyte due to the use of potentiostatic charge/discharge cycling. Both refs. [31] & [35] cycle cells galvanostatically, consistently accessing less than 90% of their theoretical initial capacity, thus leading to inconsistent results associated with accessing the full SOC. When comparing multiple different cells with presumably different cell ohmic resistances (typically membrane-dominated, especially across multiple pH values), galvanostatic cycling alone results in significantly different absolute values of accessed capacities, casting serious doubt on any cell capacity fade comparison made using such susceptible cycling techniques. Given that a proper symmetric cell begins initially at 50% SOC in the CLS and NCLS, and each cell is charged first, the first charge capacity data point is roughly half of the total capacity (i.e., the CLS is charged from 50% to 100% SOC) and the first discharge capacity data point is the total capacity (i.e. the CLS is discharged from 100% to 0% SOC). Of note in Fig. 1, initial discharge capacities of greater than 100% theoretical capacity are achieved, with increased capacity seen at increased pH – especially at pH 14 where 112% of theoretical capacity is achieved in the first discharge. If ferri-/ferrocyanide is chemically stable and these cells simply suffer from apparent capacity fade, this is an indication of the previously reported [32] pH-dependent parasitic reduction of ferricyanide to ferrocyanide. During discharge, the CLS converts ferrocyanide to ferricyanide (facilitated electrochemically by the flow cell) but an electroless reduction of ferricyanide back to ferrocyanide could continually occur in solution as long as ferricyanide is present.

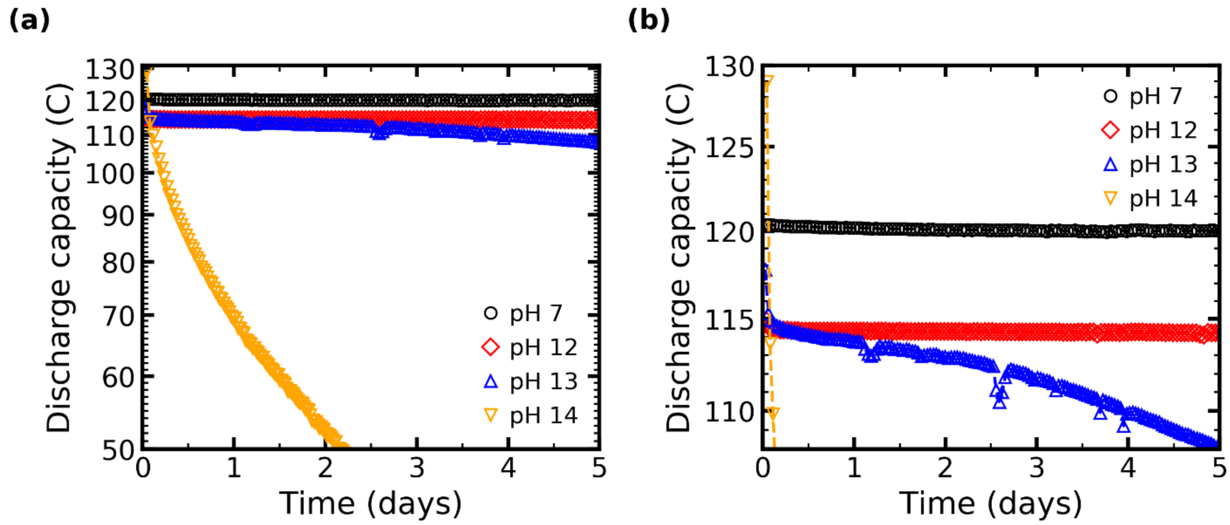

Figure 1. (a) Potentiostatic cycling of 0.1 M ferri-/0.1 M ferrocyanide at pH 7, 12, 13, and 14 in symmetric cells with SGL electrodes; pH 7 is 6.3 mL CLS vs 11.0 mL NCLS, while all other cells are 6.0 mL CLS vs 11.0 mL NCLS. (b) with zoomed in vertical scale.

Given that the reduction potential of ferri-/ferrocyanide is pH-independent, high pH leads to increased favorability of the OER in a ferri-/ferrocyanide solution. This effect can be explained by examining the Pourbaix diagram for aqueous ferri-/ferrocyanide in Fig. 2, with half reactions of interest described by equations (1) and (2). A subtle distinction to be considered is the Nernstian shift of the OER potential–pH equilibrium line as a function of oxygen partial pressure: assuming room temperature, the OER in air (21% oxygen) is shifted 10 mV more negative than standard conditions (i.e., 1 bar oxygen), and in glovebox (2 ppm oxygen) the OER is shifted 84 mV more negative than standard conditions. Thus, for a 50% SOC ferri-/ferrocyanide electrolyte, the oxidation of water accompanied by the reduction of ferricyanide to ferrocyanide is thermodynamically possible at pH >12.3 in air, or pH >11.1 in glovebox. It should be noted, however, that electrochemically, the OER is kinetically sluggish – especially on carbon electrodes [36].

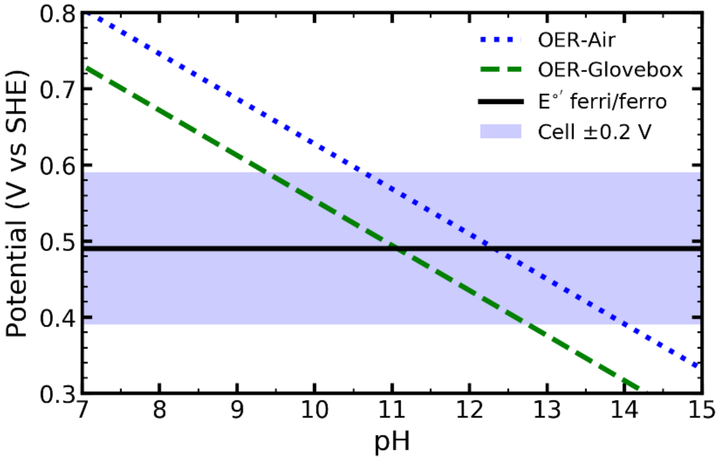

Figure 2. Pourbaix diagram of ferri-/ferrocyanide, oxygen evolution reaction (OER) in different atmospheres, and 200 mV window accessed by the symmetric cell when an initially 50% SOC solution is used as CLS and NCLS.

$$4Fe(CN)_6^{3-} + 4e^- \rightarrow 4Fe(CN)_6^{4-} \quad (1)$$

$$4OH^- \rightarrow 2H_2O + O_2 + 4e^- \quad (2)$$

When cycling a symmetric cell starting at 50% SOC in both the CLS and NCLS (i.e., identical solutions except in volume), the initial open circuit voltage is 0 V, and a voltage of ±200 mV is applied across the cell for charge/discharge in order to access over 99% of the capacity of the CLS [32]. Given that both sides of the cell contain identical concentrations of the same starting electrolytes, it is reasonable to assume that the applied potential is equally divided between CLS and NCLS i.e. 100 mV of overpotential per side (see blue shaded region of Fig. 2 denoting ±100 mV window about the formal reduction potential of ferri-/ferrocyanide, resulting from an absolute applied voltage of 0.2 V on each charge/discharge cycle). A previous report attributes the observed capacity fade to electrochemical OER occurring concurrently with ferricyanide reduction during the discharging process [34]. However, the electrochemical OER is kinetically sluggish on carbon and would proceed only when a large overpotential is applied. This is inconsistent with the results of Goulet and Aziz [32], in which fast capacity fade was still observed when pH 14 ferri-/ferrocyanide electrolytes were pumped through a cell without any electrochemical cycling, and capacity fade rates significantly decreased when electrolytes were stored out of contact with the electrodes of the cell for a period of time before cycling the cell again. The observed rapid reduction of ferricyanide in alkaline conditions is indicative of an electroless (chemical) reduction, possibly catalyzed by carbon electrodes. Taken together, these results indicate that reports of 100% capacity retention in neutral pH ferri-/ferrocyanide electrolytes are not unprecedented, as neither chemical oxidation of water by ferricyanide nor electrochemical oxygen evolution at the applied cell potentials is favored in neutral pH conditions [37]. Other examples of electroless OER facilitated by species with similar reduction potentials to ferri-/ferrocyanide include $Au(OH)_4^-$ [38], and $W(CN)_6^{3-}$ and $Mo(CN)_6^{3-}$ [39].

NMR confusion: Carbonate species vs free cyanide

In the reported claim of alkaline ferri-/ferrocyanide chemical instability, ref. [31], the supposed nail in the coffin was ^{13}C NMR detection of free cyanide. Páez *et al.* proposed that this signal arises from dissolved carbonate, not free cyanide, which they hypothesized comes from K_2CO_3 impurity present in bulk dry KOH [34]. However, while we agree that carbonate is being detected instead of free cyanide, we hypothesize that the main source of dissolved carbonate in both works is actually atmospheric in origin. ^{13}C NMR data from ref. [34] demonstrates a carbonate signal that increased in intensity as the electrolyte was cycled in an RFB over time, analogous to the results in ref. [31]. Neither report makes any mention of the use of an inert glovebox atmosphere for both flow cell cycling and ^{13}C NMR sample preparation, leading us to assume that atmospheric CO_2 could readily dissolve in the highly alkaline electrolytes as they cycled. CO_2 dissolution kinetics in alkaline aqueous solutions are known to be rapid, with the carbonate ion being the dominant carbon species at high pH, and bicarbonate ion dominating in mildly alkaline conditions. Further complicating the analysis of cycled alkaline ferri-/ferrocyanide electrolytes is the following unlucky twist of fate: in alkaline conditions, free cyanide has a ^{13}C NMR shift of 165-166 ppm [40,41], but between pH 7-14, the carbonate/bicarbonate peak ranges over 161-170 ppm, potentially overlapping the cyanide signal [42]. The range in signal shift is due to the fast equilibration of carbonate/bicarbonate which results in a single NMR peak whose chemical shift depends on the relative concentration of the two species, which is of course, a function of pH [43]. This explains the carbonate/bicarbonate peak and lack of free cyanide peak observed in ^{13}C NMR data from ref. [34], and the peak misattributed to free cyanide in ref. [31]. Results from cycled ferri-/ferrocyanide electrolytes at pH >14 also show the same issue of carbonate being mistaken for cyanide [44].

To confirm the chemical stability of alkaline ferri-/ferrocyanide electrolytes under our cycling conditions, we measured the ^{13}C NMR of the pH 14 electrolyte solutions for CLS and NCLS reservoirs before and after the cycling that showed dramatic capacity fade in Fig. 1. The spectra are reported in Fig. 3. The ^{13}C NMR measurements were conducted on electrolytes before and after cycling to detect whether cyanide anions had formed during cycling. The signal at 38.8 ppm corresponds to the internal standard DMSO, and the signal at 176.8 ppm corresponds to diamagnetic ferrocyanide. Ferricyanide is a paramagnetic species and is not detected in standard ^{13}C NMR; the presence of small amounts of ferricyanide inhibits the carbon signal from ferrocyanide, as shown in ref. [34]. Therefore, measuring ^{13}C NMR of cycled ferri-/ferrocyanide electrolytes without first ensuring a fully reduced (i.e., all ferrocyanide) sample, would likely not deliver any carbon signal. Combined with the presence of undesired dissolved CO_2 species (as described earlier) one could be led to incorrectly concluding that ferri-/ferrocyanide has fully degraded and released its cyanide ligands into solution, as we believe occurred in ref. [31]. We used a solution of 0.1 M potassium cyanide at pH 14 as a positive control, with a signal at 164.9 ppm corresponding to free cyanide anions, seen in Fig. 3c. The distinct difference in chemical shift between ferrocyanide and free cyanide indicates that the ferri-/ferrocyanide alkaline posolyte did not chemically decompose to produce cyanide anions when cycled electrochemically in a symmetric cell, in either the NCLS (Fig. 3a) or the CLS (Fig. 3b). This is consistent with recent reports [32,34] and confirms that the capacity fade observed during cell tests is only apparent and is not linked to chemical decomposition of ferricyanide. In recent work, a mechanism involving homogeneous ferricyanide reduction facilitated by cyanide oxidation to cyanate (OCN^-) was proposed [35]. Once again, the evidence for this process appears to be derived from misinterpreted ^{13}C NMR spectra, where an NMR peak near 167 ppm is attributed to cyanate (normally found near 129 ppm [45,46]) when it is due simply to free cyanide that had been added to solution. Given that the electroless ferricyanide reduction is already being facilitated by the electroless OER, the presence or absence of cyanide in solution would not affect the final result of conversion to ferrocyanide. Furthermore, ref. [35] claims that ammonia/ammonium was detected in ferri-/ferrocyanide electrolytes, thus proving their hypothesized mechanism of electroless ferricyanide reduction via cyanide oxidation to cyanate, which further hydrolyzes to ammonium. We offer an alternative explanation for these results. The method of adding strong acid to a solution of ferri-/ferrocyanide to trap ammonia (which evolves under the proposed mechanism) leads to a self-fulfilling prophecy: strong acid could in fact both release cyanide ligands from ferri-/ferrocyanide and hydrolyze the resulting free cyanide to ammonium formate. Acid-mediated hydrolysis of cyanide to ammonium formate is well documented [47-49] thus the proposed chemical reduction of cyanide to cyanate, further hydrolyzed to ammonia, may be incorrect in ref. [35]. This would explain the eventual detection of ammonia/ammonium and formate through the combination of *ex situ* ^{1}H NMR/^{13}C NMR/GC-FID results in ref. [35]. Hydrolysis of cyanide to ammonium can also be expedited by heating the solution [50], and ref. [35] detected ammonia by using GC-FID which heats the solution to several hundred degrees Celsius. Furthermore, ref. [35] did not state that the pH of all solutions tested by GC-FID are the same, thus any trend of ammonia concentration cannot necessarily be determined, as ammonia volatility is extremely pH-dependent.

In Fig. 3, the absence of a signal from either the cycled CLS or NCLS electrolyte between 161-170 ppm indicates that we have prevented absorption of atmospheric CO_2, which would result in dissolved carbonates and obfuscate any detection of free cyanide. Given that we do not observe free cyanide in fresh electrolytes, or cycled electrolytes exhibiting large apparent capacity fade, our results clearly undermine the proposed mechanisms in [31] and [35], and are a strong indication that alkaline ferri-/ferrocyanide electrolytes are chemically stable for RFB applications.

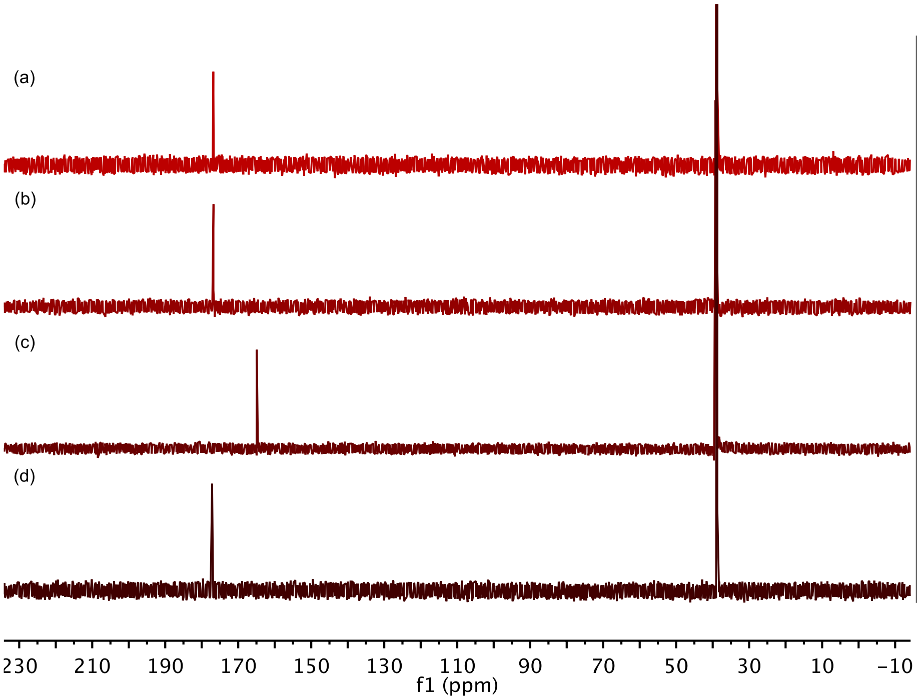

Figure 3. ^{13}C NMR measurements of (a) Electrolyte from NCLS of 0.1 M ferri-/0.1 M ferrocyanide pH 14 symmetric cell with SGL electrodes. Electrochemically cycled for 7 days, and then fully reduced to ferrocyanide; (b) Electrolyte from CLS of 0.1 M ferri-/0.1 M ferrocyanide pH 14 symmetric cell with SGL electrodes. Electrochemically cycled for 7 days, and then fully reduced to ferrocyanide; (c) 0.1 M potassium cyanide at pH 14; (d) 0.1 M ferrocyanide at pH 14, uncycled.

Carbon electrode-catalyzed electroless redox

To quantitatively probe the stability of ferricyanide and its previously hypothesized interaction with porous carbon electrodes [32], we used UV-Vis spectrophotometry to measure total ferricyanide and total iron concentrations over time in quiescent solutions with and without SGL carbon electrodes. In Figure 4 we report the resulting changes in ferricyanide and total iron concentration for a series of pH 14 solutions stored either in contact or out of contact with SGL electrodes. The data in Fig. 4 indicate that the total concentration of iron remains constant during both experiments, while the ferricyanide concentration decreases to almost zero in less than a week when the solution is in contact with the electrode. This demonstrates that there is a direct interaction between the carbon surface and ferricyanide. At high pH, the carbon electrode appears to enhance the rate of electroless ferricyanide reduction to ferrocyanide facilitated by the chemical OER, as previously reported [32]. However, a relatively slow chemical reduction of ferricyanide was still observed in solutions that were not in contact with the carbon electrodes, at a rate of 3%/day for a 3 mL sample of 0.5 mM ferricyanide at pH 14. In the absence of electrode contact, the rate of homogeneous ferricyanide reduction will ultimately set a pH-dependent upper limit on the lifetime for any RFB configuration. Understanding how this rate depends on pH, concentration of ferri-/ferrocyanide, oxygen partial pressure in the headspace, and mixing properties of the electrolyte, is an important direction for future work.

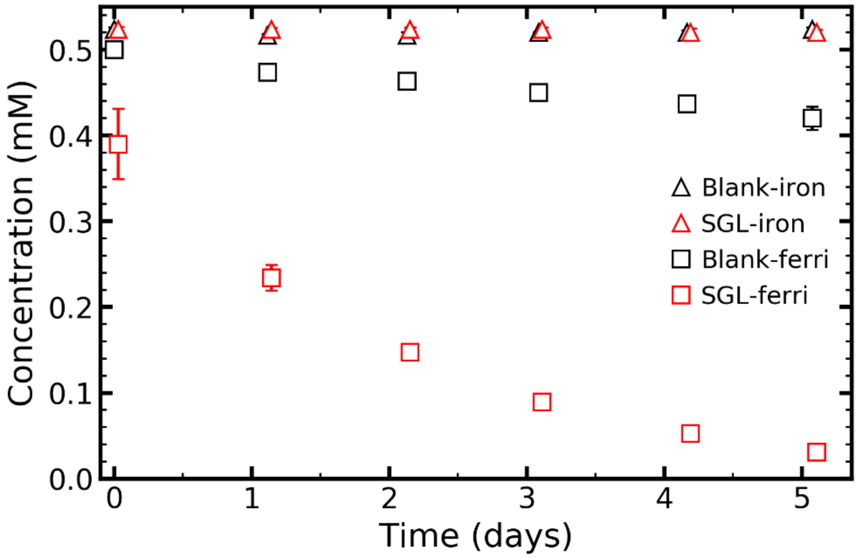

Figure 4. UV-Vis measured time-dependence of ferricyanide and total iron concentration in 3 mL of 0.5 mM ferricyanide pH 14 solution in contact and out of contact with 4 mm × 4 mm SGL electrode. Solutions were stored in glass vials.

In the supplementary information (see Fig. S1) we report the same experiment done using more oxygen permeable polypropylene vials and that those solutions exhibited faster reduction of the ferricyanide anions due to evolved oxygen escaping the vials more quickly. This suggests that the electroless OER (equation 2) raises the oxygen partial pressure in the head space, which acts to suppress the electroless OER rate unless O_2 escapes from the head space. To test this hypothesis, we employed gas chromatography-mass spectrometry (GC-MS) to detect the formation of O_2. Three samples were prepared in glovebox: (a) 5 mL of 1 M KOH; (b) 5 mL of 0.25 M ferricyanide in 1 M KOH; (c) 5 mL of 0.25 M ferricyanide in 1 M KOH soaking a 5 cm^2 SGL carbon electrode. All solutions were sealed in 10 mL air-tight headspace vials for GC-MS measurements. Fig. S2 shows that an oxygen signal was detected from sample (b) and (c), which is consistent with equations (1) and (2) stating that hydroxide is oxidized to O_2 while ferricyanide is reduced to ferrocyanide. Furthermore, a stronger oxygen signal (higher signal/noise ratio) is detected from sample (c), implying that the carbon electrode plays a role in catalyzing this chemical redox reaction. Additionally, the ^{13}C NMR spectrum of post-cycled ferri-/ferrocyanide electrolyte (Fig. 3a & 3b) does not show any side peaks, indicating that the SGL carbon electrode was not oxidized to any soluble carbonaceous species such as carbonate (given the alkaline conditions), thus ruling out carbon electrode oxidation by ferricyanide. Therefore, both *in situ* (cell cycling) and *ex situ* (^{13}C NMR, UV-Vis, GC-MS) experiments support the hypothesis of a pH-dependent electroless reduction of ferricyanide accompanied by electroless OER, which can be further accelerated by carbon electrodes. A recent report [35] proposing electroless reduction of ferricyanide facilitated by free cyanide oxidation did not detect evolved O_2 in ferri-/ferrocyanide electrolytes but one possible reason for this is that their GC experiments were performed only on post-cycled electrolytes, when electroless OER may already have ceased after reaching equilibrium. It is understandable that with a continuously flowing electrolyte, unsealed reservoir headspace, and gas permeable flow cell equipment, small amounts of oxygen evolution could go unnoticed and escape from lab-scale flow cells.

Electrode surface area

The results of the previous section would indicate a potential issue for RFB design when employing ferri-/ferrocyanide electrolytes and carbon electrodes. To explore the effect of electrode surface area, we utilized a porous electrode with nearly five times less surface area, the HCBA woven carbon cloth. Symmetric cell cycling of 0.1 M ferri-/0.1 M ferrocyanide solutions at different pH with HCBA electrodes is shown in Fig. 5, with the pH 14 SGL cycling data from Fig. 1 included as a comparison. The plotted discharge capacities of HCBA cells in Fig. 5a represent 250, 255, and 201 cycles for pH 12, 13, and 14, respectively. Once again, each symmetric cell in Fig. 5 initially accesses >99% of the theoretical capacity of the CLS electrolyte due to the use of potentiostatic charge/discharge cycling. As seen in Fig. 1, cells using SGL electrodes often demonstrated initial discharge capacities greater than 100% theoretical capacity, with increased initial capacity seen at increased pH, consistent with a chemical reduction of ferricyanide to ferrocyanide. In the HCBA cells of Fig. 5, this effect is no longer seen in the discharge capacity data. During symmetric cell cycling using SGL electrodes, a fast apparent capacity fade rate of roughly 20%/day was observed at pH 14, but when cells were cycled using HCBA electrodes and pH 14 conditions only a minimal 0.1%/day apparent capacity fade rate was measured. Table 1 illustrates the increase in instantaneous apparent capacity fade rate with increasing pH for the symmetric cells of Figs. 1&5. These results imply that the coupled electroless ferricyanide reduction/OER reaction is enhanced by carbon electrode surface area, and therefore influences apparent capacity fade rates in symmetric cells.

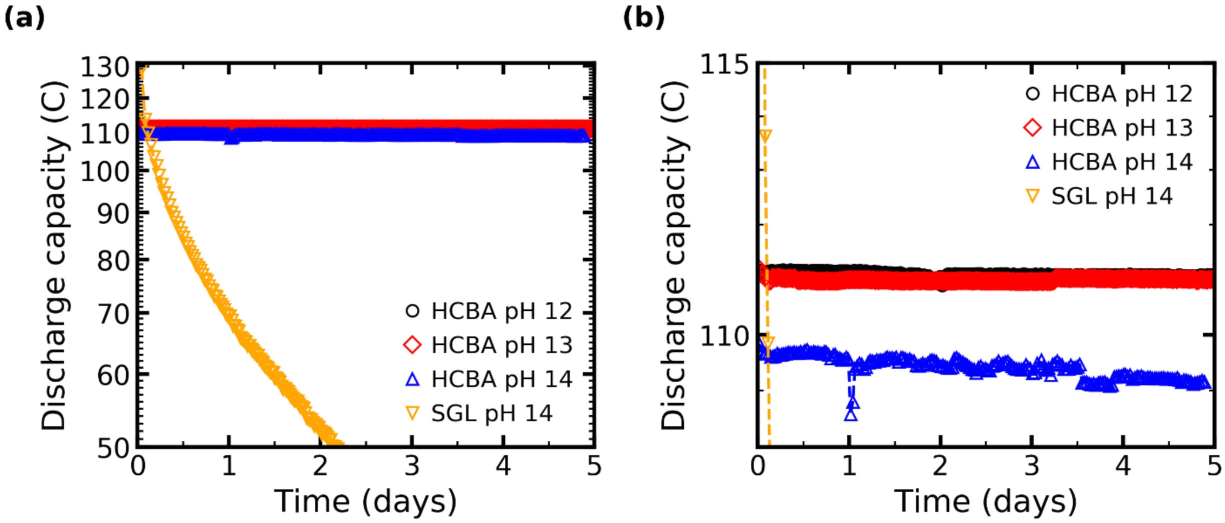

Figure 5. (a) Potentiostatic cycling of 0.1 M ferri-/0.1 M ferrocyanide at pH 12, 13, and 14 in symmetric cells with HCBA electrodes; pH 12 and 13 are 5.8 mL CLS vs 11.0 mL NCLS, pH 14

is 5.7 mL CLS vs 11.0 mL NCLS. Cell data for pH 14 with SGL electrodes from Fig. 1 is included as comparison. (b) with zoomed in vertical scale.

Table 1. Instantaneous apparent capacity fade rates of 0.1 M ferri-/0.1 M ferrocyanide symmetric cells, nominally 6 mL CLS vs 11 mL NCLS, cycled in glovebox.

pH	**Instantaneous apparent capacity fade rate (%/day)**	
	SGL	**HCBA**
7	none	--
12	<0.01	<0.01
13	1.4	0.01
14	20	0.1

We also measured the pH, before and after cycling, of the CLS electrolytes in SGL and HCBA cells, reported in Fig. 6 as total decrease in hydroxide concentration. 0.1 M ferro/0.1 M ferricyanide solutions at the given pH values were used as controls to monitor the coupled electroless ferricyanide reduction/OER without enhancement from contact with carbon electrodes, all kept and measured in glovebox. At each starting pH, the symmetric cells using SGL electrodes demonstrated larger loss of hydroxide than HCBA cells, but the use of either electrode led to a larger decrease in hydroxide concentration than the respective blank. For cycled electrolytes at pH 12, 13, and 14, the SGL cells experienced a decrease in initial hydroxide concentrations of approximately 80%, 60%, and 20%, respectively.

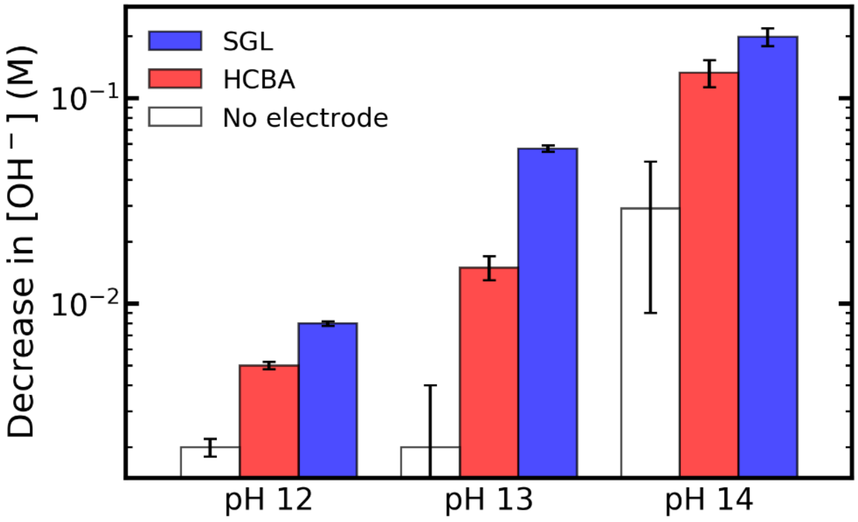

Figure 6. Total decreased hydroxide concentration in the CLS of the symmetric cells from Figs. 1&5, measured after 5 days of cycling in a glovebox. ‘No electrode’ is a 0.1 M ferro/0.1 M ferricyanide solution at the given pH, identical to the starting CLS of each cell, left stirring in glovebox but without any contact with a carbon electrode.

^{13}C NMR measurements were performed for cycled and uncycled pH 14 electrolytes when HCBA was used as the electrode (analogous to SGL measurements seen in Fig. 3). ^{13}C NMR spectra of electrolytes from the HCBA cell are shown in Fig. S4. Consistent with the results from SGL electrodes, we do not detect any formation of free cyanide in electrolytes cycled with HCBA electrodes, providing further proof that the capacity fade observed during cell tests is only apparent and is not linked to chemical decomposition of ferri-/ferrocyanide. Dissolved carbonates were not detected either, ruling out any process involving ferricyanide reduction facilitated by carbon electrode corrosion to dissolved inorganic species in alkaline conditions. UV-Vis measurements of total ferricyanide and total iron concentrations over time in pH 14 electrolyte-soaked HCBA electrodes (analogous to experiments performed in Fig. 4 for SGL electrodes) can be seen in Fig. S5. A trend of increased ferricyanide reduction in the presence of carbon electrodes was again observed. However, it should be noted that the rate of ferricyanide reduction in these *ex situ* measurements cannot easily be compared to the observed apparent fade rates in cell cycling because the UV-Vis measurements are in quiescent solutions (compared to constant electrolyte flow in cells) and the act of electrochemically charging/discharging electrolytes in symmetric cells enforces a non-linear (electrochemical) replenishment of a reactant i.e., ferricyanide. Furthermore, we cannot compare the rates of ferricyanide reduction between the two electrodes in the *ex situ* UV-Vis experiments, because the use of quiescent solutions results in diffusion-limited reactions controlled by the intricate porous structures of the electrodes, which differ considerably.

To compare the available active sites of SGL and HCBA electrodes that enhance the coupled electroless reduction of ferricyanide and OER requires the combined characterization of hydraulic permeability and mass transport within the electrodes, the effect (if any) of electrode surface functional groups and/or doping on liquid/gas interactions, O_2 diffusion in the electrode, electrode compression, and electrochemically active surface area for the desired ferri-/ferrocyanide redox reaction, and is beyond the scope of this work [51-56]. As a simplification, we report BET surface area from gas adsorption measurements in the Table S1 as an estimate of maximum available surface area for enhancement of the electroless process. We observe SGL to have nearly an order of magnitude larger specific surface area than HCBA. An area for future work includes the quantification of such a unique three-phase interaction for the electroless process, and how it couples to mass transport within porous/woven carbon electrodes and electrochemically-driven redox reactions within an RFB.

Another issue with the SGL carbon electrodes is the graphitic binder that holds the intricate system of carbon fibers in place, enabling the electrode to have such large surface area. The binder contains no fluorinated or sulfonated polymers in the matrix, as is typically found in electrodes used for fuel cells. This is contrasted by the HCBA electrodes fabricated by inter-weaving carbon fibers to provide mechanical strength without the need for a binder. SEM images of both electrodes are shown in Fig. S6, along with EDS analysis with the elemental composition for SGL (Fig. S7) and HCBA (Fig. S8). Because of the manufacturing process, the mats of HCBA electrodes are thicker than the SGL, producing electrode mats with lower surface areas. We find that when cycling pH 14 ferri-/ferrocyanide electrolytes in symmetric cells using SGL electrodes, loss of carbon fibers can occur during cycling and can be seen by the change in color of the electrolyte solutions, which become darker. When left in quiescence for a few days after cycling, black fibrous deposits became apparent on the bottom of the electrolyte reservoirs, as shown in Fig. S9, indicative of fiber/binder removal from the electrode. The use of high surface area porous electrodes with binders complicates matters as the OER process can be mechanically destructive (gas generation in liquid-filled pores), causing the binder to disintegrate over time and releasing electrode fibers. SGL is a gas diffusion electrode (GDE) optimized for gas flow in polymer electrolyte fuel cells, rather than liquid flow in an RFB, thus mechanical removal of degraded binder facilitated by constant electrolyte flow through the electrodes could occur. Much of the work in AORFBs has been built using the adopted architecture of fuel cells, especially the use of GDEs to provide high active surface area to facilitate the electrochemistry of dissolved redox-actives [57]. Only recently has it been shown that carbon cloth electrodes may provide improved performance for RFBs in terms of electrochemical and hydraulic performance [52,53,58]. Achieving the lowest active surface area electrode that still provides the best overall performance would minimize the effect of the electrode-enhanced electroless ferricyanide reduction, while possibly also minimizing electrode materials costs. An important avenue for future work is correlating the difference in apparent capacity fade rates between electrodes with characteristics such as the electrode active surface area in contact with the electrolyte and the electrode mass transport properties.

Apparent capacity fade

To distinguish coulometrically between irreversible chemical decomposition and apparent capacity fade due to electrode-enhanced electroless ferricyanide reduction, a 0.1 M ferri-/0.1 M ferrocyanide pH 14 symmetric cell with SGL electrodes was cycled for approximately four days, resulting in significant apparent capacity fade, as seen in Fig. 7. Electrochemical cycling was then paused, and the NCLS was replaced with a fresh electrolyte identical to the starting NCLS i.e., 50% SOC, 0.1 M ferri-/0.1 M ferrocyanide at pH 14. Electrochemical cycling was then restarted for two days before a second NCLS refresh occurred. When considering the initial discharge of >100% theoretical capacity (explained above, seen in Fig. 1), each successive NCLS refresh allowed for full capacity recovery in the CLS. Each successive run demonstrated a significant decrease in the instantaneous apparent capacity fade rate: 20%/day during initial cycling, 5%/day after the first NCLS refresh, and 0.1%/day after the second NCLS refresh. We attribute this change in capacity fade primarily to the continuous decrease in CLS pH due to electroless OER, the rate of which decreases with decreased pH. Although we refresh the NCLS with a new pH 14 solution, the NCLS does not access the SOC extreme where ferricyanide is highest in concentration as often as the CLS. The loss of SGL fibers due to mechanical degradation of the binder, which reduces active surface area that can enhance the electroless ferricyanide reduction, may also contribute to the decreased apparent capacity fade rate to a lesser degree. This experiment also highlights the importance of checking whether observed capacity fade is real or apparent, by refreshing or adding additional NCLS electrolyte after significant capacity loss has been observed. This rule applies to both full cells and symmetric cells. The data in Fig. 7 prior to the first NCLS refresh are similar to previously published [31,35] alkaline ferri-/ferrocyanide cells where the authors concluded in each case that extreme capacity fade was due to irreversible chemical degradation, rather than checking whether cell unbalancing had occurred and all initial capacity actually remained. We also carried out a similar experiment with a 0.05 M ferri-/0.05 M ferrocyanide pH 14 electrolyte, and once again were able to fully achieve the initial CLS capacity after significant apparent capacity fade. We refer the reader to Fig. S10 for details.

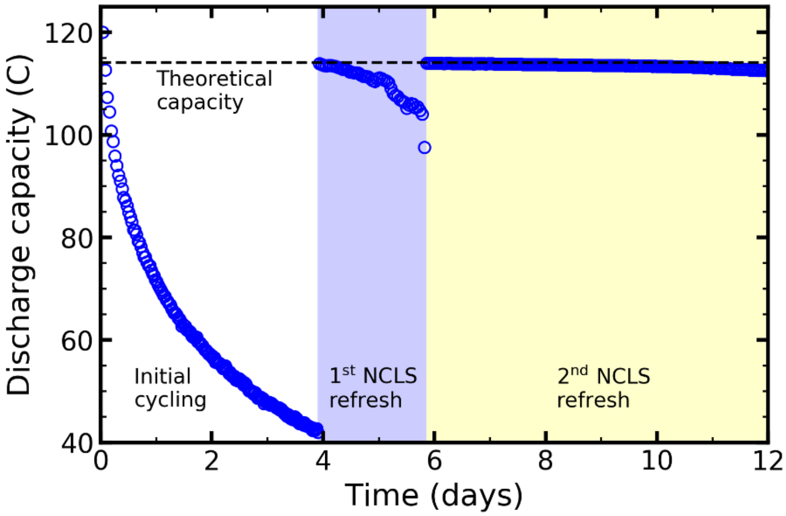

Figure 6. Potentiostatic cycling of a 0.1 M ferri-/0.1 M ferrocyanide pH 14 symmetric cell (6 mL CLS vs 11 mL NCLS) with SGL electrodes. The NCLS was replaced after approximately 4 days, and 6 days, with 11 mL of fresh 50% SOC electrolyte. The CLS is discharged prior to NCLS replacement.

We next quantified the effect of CLS electrolyte refreshment, identical to the experiment shown in Fig. 7, but this time replacing the initial CLS after significant apparent capacity fade had occurred. Once again, a 0.1 M ferri-/0.1 M ferrocyanide pH 14 symmetric cell with SGL electrodes was cycled, as seen in Fig. 8. After 7 days and significant apparent capacity fade, electrochemical cycling was paused with the CLS discharged, and the CLS was replaced with a fresh electrolyte identical to the starting 50% SOC CLS. After another 7 days of cycling, a second CLS refreshment occurred. Given that each refresh introduces a new 6 mL CLS with slightly different capacity due to uncertainty in aliquoting, we plot normalized discharge capacity (defined as discharge cycle capacity normalized by discharge capacity of the first cycle) for each new CLS used. Once again, each successive CLS refresh demonstrated a significant decrease in the instantaneous apparent capacity fade rate. In this case however, the starting NCLS is used for the entire 21 days of cell cycling. During this time, there is a continuous decrease in NCLS pH due to the electroless OER. The electroless process is pH-dependent, with a decreasing rate with decreased pH, and so the rate at which the NCLS can unbalance the cell slows over time. Before each CLS refresh, the cell is paused with the CLS in a discharged (oxidized) state, meaning that the NCLS is in a charged (reduced) state containing mainly ferrocyanide. The electroless reduction of ferricyanide continues to create more ferrocyanide in the NCLS as well. This means that when a fresh CLS is introduced and charged up (ferricyanide in the CLS electrochemically converted to ferrocyanide), the NCLS has a larger available SOC range (more available ferrocyanide to electrochemically convert to ferricyanide) than before and thus the cell takes longer to become unbalanced, resulting in a slower apparent capacity fade rate. This process occurs again after another CLS refresh, albeit even slower.

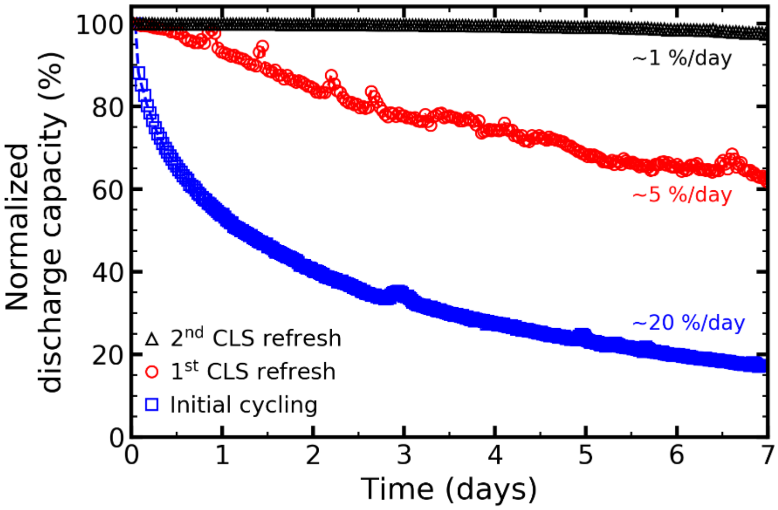

Figure 7. Potentiostatic cycling of a 0.1 M ferri-/0.1 M ferrocyanide pH 14 symmetric cell (6 mL vs 11 mL) with SGL electrodes. After 7 days of cycling (blue squares), the CLS was replaced with 6 mL of fresh 50% SOC electrolyte and cycled for 7 days (red circles). This CLS replacement was repeated a second time and again cycled for 7 days (black triangles).

The experiments of Figs. 7 and 8 demonstrate the ways in which measured capacity fade can be apparent but not real, and the importance of understanding the accessible SOC range in both the CLS and the NCLS. First, capacity in the CLS can be fully accessed only if there is enough accessible capacity in an NCLS. By accessible, we mean enough reduced species in the NCLS to be oxidized so that oxidized species in the CLS can be reduced on charging, and vice versa for discharging. Unwanted shifts in SOC, even if only occurring in the NCLS, can result in a smaller accessible range of SOC in the CLS. For example, a very large NCLS at an extreme SOC (i.e., near 0% or 100%) may still result in the inability to access all capacity in a much smaller CLS, depending on the CLS SOC. Thus, large total capacity differences between CLS and NCLS can provide a false sense of security in the ability of a cell to fully access the capacity of a CLS. It is for this very reason that all our symmetric cells used for standard characterization of capacity fade rates in new redox-active molecules begin with both CLS and NCLS at 50% SOC and include an adequate volume excess in the NCLS. Other proposed half-cell configurations do not provide this safety buffer, and their use has resulted in the misinterpretation of apparent capacity fade rates as real capacity fade rates [31,35,59].

The effect of the electroless ferricyanide reduction at pH 14 with SGL electrodes was then evaluated in terms of flow battery relevant design metrics, such as electrode geometric surface area, electrolyte volumes in the CLS and NCLS, and starting concentration of ferri-/ferrocyanide. We report the observed apparent capacity fade rates in symmetric cells as a function of the initial concentration of ferri-/ferrocyanide (all cells begin with 50% SOC electrolytes, 6 mL CLS vs 11 mL NCLS) in Fig. 9a. In symmetric cells with low concentration of ferri-/ferrocyanide, we see extremely rapid apparent capacity fade due to the large ratio of carbon electrode active surface area to molarity of ferri-/ferrocyanide in each electrolyte reservoir. With both CLS and NCLS experiencing fast electroless ferricyanide reduction, cells become unbalanced quickly, demonstrating rapid apparent capacity fade. Given the cell configuration (total electrode area, reservoir volumes) used in Fig. 9a, apparent capacity fade rates are minimized at ferri-/ferrocyanide concentrations greater than 150 mM each. Fig. 9b demonstrates the effect of increased electrode surface area on the apparent capacity fade rate, in cells containing a fixed electrolyte concentration (0.1 M ferri-/0.1 M ferrocyanide, at pH 14) configured as 12 mL CLS vs 22 mL NCLS, with varying number of 5 cm^2 layers of SGL electrodes on both sides of the symmetric cell. We see a similar trend to that of changing the ferri-/ferrocyanide concentration: as the ratio of carbon electrode active surface area to concentration of ferri-/ferrocyanide increases (i.e., more electrode layers for a fixed ferri-/ferrocyanide concentration), the apparent capacity fade rate increases. From Fig. 9, we see that apparent capacity fade rates are not just affected by ferri-/ferrocyanide concentrations but, most importantly, total molarity of ferri-/ferrocyanide per electrode surface area. Commercial scale AORFBs built for long duration energy storage would likely employ very large electrolyte volumes and optimal active species concentrations for high energy density, and thus will have very small electrode active area to mols of ferri-/ferrocyanide ratios, thereby minimizing apparent capacity fade rates (if any) attributed to the posolyte chemistry. Minimization of such apparent fade rates can already be seen in numerous reports of extremely low capacity fade rates of negolyte chemistries cycled against alkaline ferri-/ferrocyanide posolytes with very small electrode area to mols ferri-/ferrocyanide ratios [8,10,13,14,60,61].

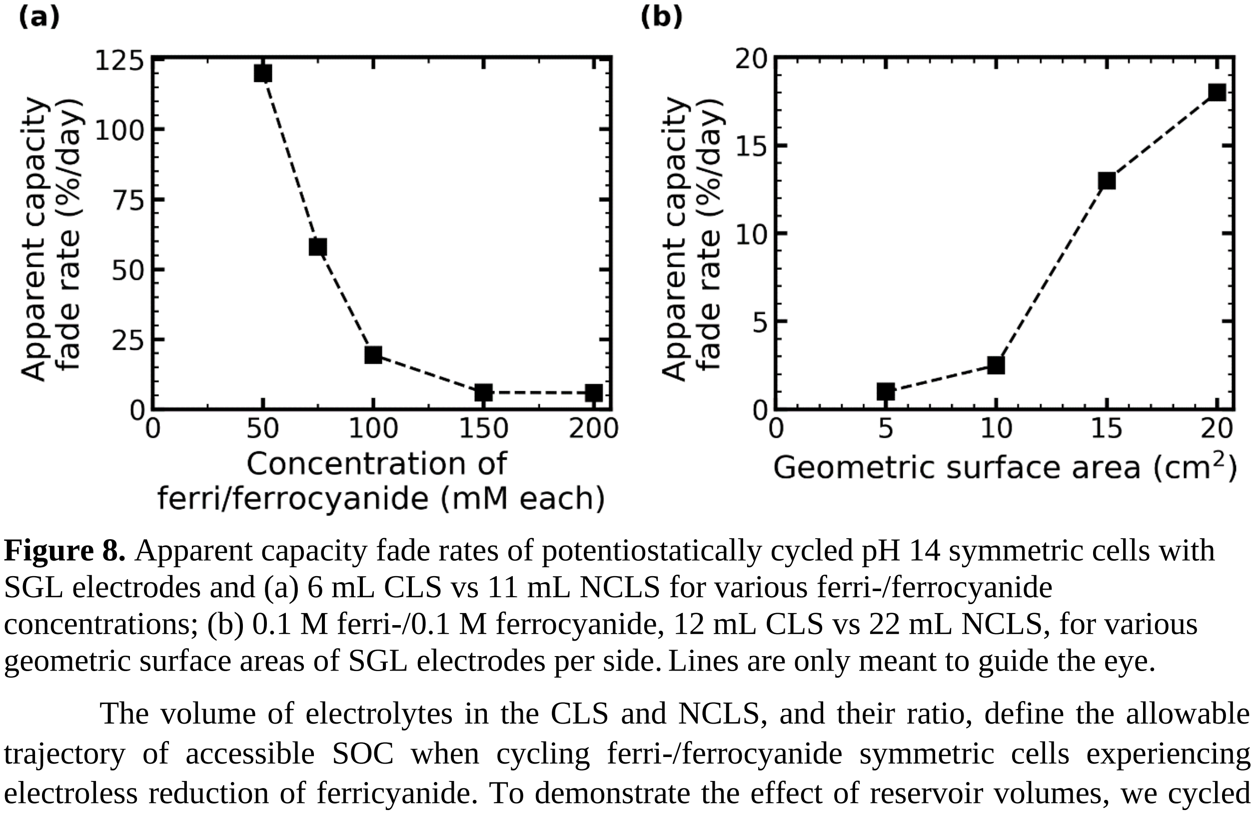

Figure 8. Apparent capacity fade rates of potentiostatically cycled pH 14 symmetric cells with SGL electrodes and (a) 6 mL CLS vs 11 mL NCLS for various ferri-/ferrocyanide concentrations; (b) 0.1 M ferri-/0.1 M ferrocyanide, 12 mL CLS vs 22 mL NCLS, for various geometric surface areas of SGL electrodes per side. Lines are only meant to guide the eye.

The volume of electrolytes in the CLS and NCLS, and their ratio, define the allowable trajectory of accessible SOC when cycling ferri-/ferrocyanide symmetric cells experiencing electroless reduction of ferricyanide. To demonstrate the effect of reservoir volumes, we cycled 0.1 M ferri-/0.1 M ferrocyanide pH 14 electrolytes in cells with SGL electrodes at multiple CLS and NCLS volume configurations. Fig. 10a demonstrates the effect on apparent capacity fade rate of varying CLS volumes for a fixed NCLS volume. We first note that apparent capacity fade rates increase as CLS volumes increase, thus a smaller difference between volumes of the CLS and NCLS leads to faster apparent capacity fade rates. This trend occurs due to the NCLS having to swing to larger SOC extremes to enable access to CLS capacity, based on the difference between the volumes of the two reservoirs, and the volume of the CLS itself. The deeper the SOC swings in the NCLS, the larger the concentration of electrochemically generated ferricyanide will be available, leading to a faster rate of electroless reduction of ferricyanide, furthering cell unbalancing. Fig. 10b demonstrates the effect on apparent capacity fade rate in cells with a fixed CLS volume of 4 mL, but varying NCLS volumes. Once again, we see increasing apparent capacity fade rates when the volume difference between CLS and NCLS is decreased, due to the larger SOC swing that must occur in a smaller NCLS to be able to access capacity in the CLS. Of the five symmetric cells shown in Fig. 10b, it was also observed that the color of the CLS was progressively darker going from the cell with smallest NCLS (largest apparent fade) to the cell with largest NCLS (lowest apparent fade). This could be explained by the fact that the lowest apparent capacity fade cell allows for the deepest SOC access of its CLS, due to its large NCLS, thus enabling maximum amounts of electroless ferricyanide reduction/OER while the cell is electrochemically cycled. Increasing amounts of OER with SGL electrodes will lead to significant mechanical degradation of the electrodes, as described above, thus leading to a darkening of the CLS electrolyte.

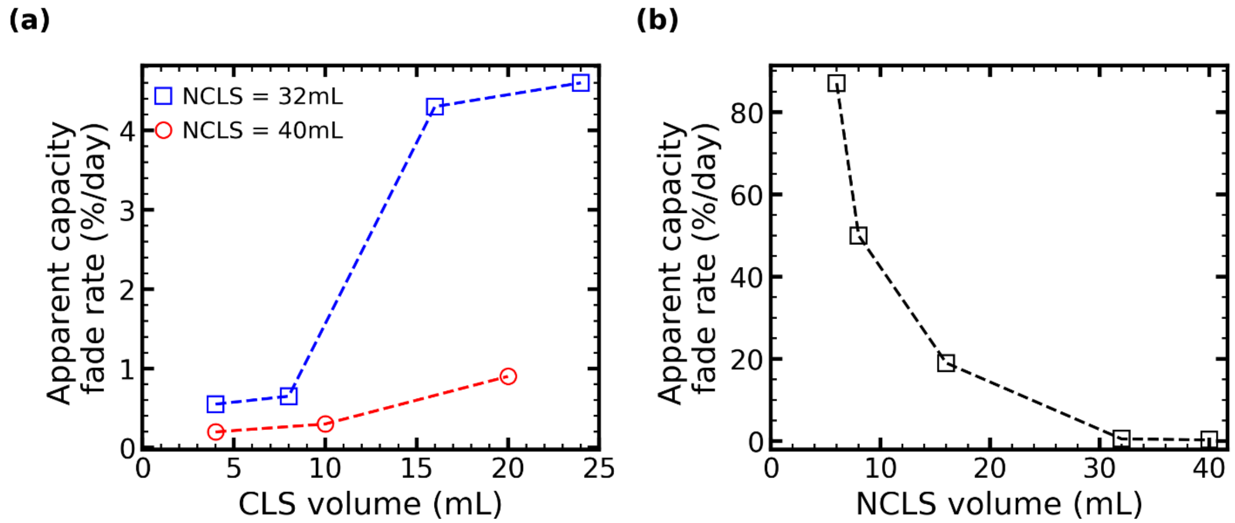

Figure 9. Apparent capacity fade rates of potentiostatically cycled 0.1 M ferri-/0.1 M ferrocyanide pH 14 symmetric cells with SGL electrodes and (a) fixed NCLS volumes; (b) fixed 4 mL CLS volume. Lines are only meant to guide the eye.

Results that follow the trends of the fixed-volume CLS/NCLS experiments are shown in Fig. 11 where we report the effect of the NCLS:CLS volume ratio on apparent capacity fade. As before, we cycled 0.1 M ferri-/0.1 M ferrocyanide pH 14 electrolytes in cells with SGL electrodes at multiple CLS and NCLS volume configurations, now plotted considering the volume ratio of the two reservoirs (some data from above figures is included here). The trends from Fig. 10 still apply, but we can now see a shifting of the CLS volume – apparent capacity fade trend with volume ratio. As the NCLS:CLS volume ratio increases, apparent capacity fade rates decrease for a given CLS volume due to the additional capacity in the NCLS allowing for deeper SOC accessing of the CLS before unbalancing occurs. Deeper SOC accessing will provide more measured capacity. Cells with the smallest volume CLS have the largest ratio of carbon electrode surface area to moles of ferricyanide, thereby exacerbating the electroless parasitic process that leads to rapid unbalancing. By varying CLS and NCLS volumes, and their ratio, we demonstrate that an apparent capacity fade rate in ferri-/ferrocyanide symmetric cells is essentially an engineered quantity i.e., an apparent fade rate depends on the choice of cell geometry (electrode surface area, volumes of CLS and NCLS, volume ratio NCLS:CLS) and electrolyte composition (pH, starting concentration of ferri-/ferrocyanide) and thus any fair comparison of apparent fade rates in ferri-/ferrocyanide symmetric cells must include a description of all such flow battery parameters.

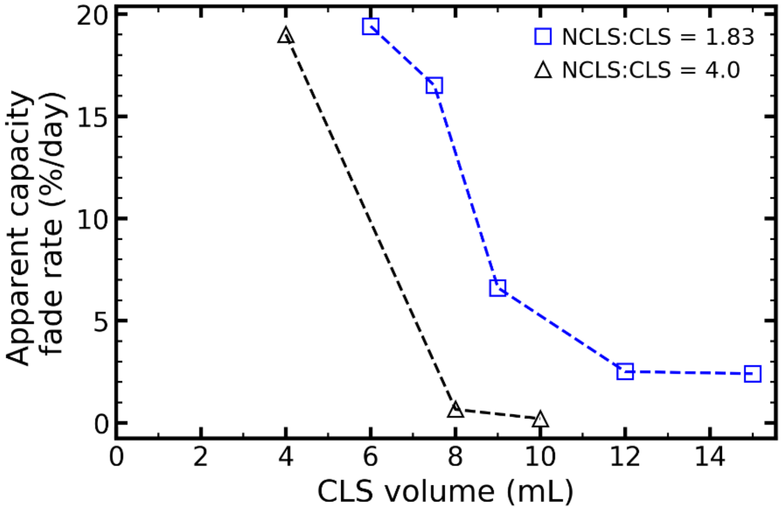

Figure 11. Apparent capacity fade rates of potentiostatically cycled 0.1 M ferri-/0.1 M ferrocyanide pH 14 symmetric cells with SGL electrodes and fixed NCLS:CLS volume ratios. Lines are only meant to guide the eye.

Conditions enabling the practical use of ferro/ferricyanide in AORFBs

Based on the experiments reported here and those in refs. [31,32,34,35], we offer the following observations enabling practical utilization of alkaline ferri-/ferrocyanide electrolytes in AORFBs:

a. For a 50% SOC electrolyte, the electroless reduction of ferricyanide via electroless OER is thermodynamically unfavorable below pH 11.1 in a glovebox and pH 12.3 in air. However, given the Nernstian shift in potential as a function of SOC, lower pH electrolytes may still enable small amounts of electroless ferricyanide reduction/OER at SOC extremes.
b. The electroless reduction of ferricyanide could be limited by maintaining high oxygen partial pressure in the reservoir headspace or by sealing the headspace to permit the partial pressure to build during use. However, one must be careful to not simply open the

headspace to air containing CO_2, as this would decrease electrolyte pH and introduce carbonates.

c. At pH 14, the electrode-catalyzed rate at which ferricyanide converts to ferrocyanide through electroless reduction via OER decreases as the ratio of the total number of ferricyanide ions to the electrode surface area increases. Consequently, we anticipate that this effect should be negligible with the large electrolyte volumes and energy densities required for practical flow battery installations with energy/power ratios of several hours.

d. Carbon electrodes with less binder, or less surface area, should be less active in promoting parasitic reduction of ferricyanide.

e. If, in the worst-case scenario, parasitic reduction of ferricyanide is unavoidable in a given system architecture, then it may be feasible to use rebalancing techniques such as electrochemical oxidation coupled with hydrogen evolution or the oxygen reduction reaction[62], as there is no loss of the ferri-/ferrocyanide redox-active species.

Conclusions

We demonstrate that in the dark/in diffuse indoor light, ferri-/ferrocyanide is chemically stable in highly alkaline electrolytes. It is determined that a pH-dependent electroless reduction of ferricyanide to ferrocyanide, via OER, occurs in alkaline electrolytes. The rate of this electroless parasitic reaction can also be enhanced by carbon electrode active area. Symmetric cell cycling experiments show that apparent capacity fade arises from the electroless process, taking the SOC of the CLS and NCLS out of balance, thereby decreasing the accessible capacity of the system. The apparent capacity loss can be completely recovered by refreshing the NCLS and/or various rebalancing techniques. We also present evidence to support our arguments that refs. [31,35] have incorrectly attributed apparent capacity fade to the chemical degradation of ferri-/ferrocyanide and assigned a carbonate peak to free cyanide. We show that symmetric cell unbalancing occurs due to electroless OER rather than electrochemical OER as previously hypothesized in ref. [34]. These results highlight the importance of an engineered atmosphere when cycling AORFBs, not only to prevent the oxidation of low-potential negolyte species by oxygen, but also to prevent CO_2 dissolution and the resulting pH variations in alkaline electrolytes. Our experiments further demonstrate that the apparent capacity fade rate at pH 14 decreases as the ratio of the total number of ferricyanide ions to the electrode surface area increases. We reveal how the apparent capacity fade rate of an alkaline ferri-/ferrocyanide symmetric cell is manipulated by the choice of electrode area, reservoir volumes, pH, and concentration. Based on these results, we anticipate that the impact of electrode-catalyzed parasitic ferricyanide reduction at tested pH values up to 14 should be negligible in a commercial scale application with the large electrolyte volumes required for RFB installations with energy/power ratios of several hours, cycling each day. These results should prevent the AORFB community from being misled into rejecting ferri-/ferrocyanide as a competitive posolyte species in alkaline conditions.

Figure descriptions

Figure 10. (a) Potentiostatic cycling of 0.1 M ferri-/0.1 M ferrocyanide at pH 7, 12, 13, and 14 in symmetric cells with SGL electrodes; pH 7 is 6.3 mL CLS vs 11.0 mL NCLS, while all other cells are 6.0 mL CLS vs 11.0 mL NCLS. (b) with zoomed in vertical scale.

Figure 11. Pourbaix diagram of ferri-/ferrocyanide, oxygen evolution reaction (OER) in different atmospheres, and 200 mV window accessed by the symmetric cell when an initially 50% SOC solution is used as CLS and NCLS.

Figure 12. ^{13}C NMR measurements of (a) Electrolyte from NCLS of 0.1 M ferri-/0.1 M ferrocyanide pH 14 symmetric cell with SGL electrodes. Electrochemically cycled for 7 days, and then fully reduced to ferrocyanide; (b) Electrolyte from CLS of 0.1 M ferri-/0.1 M ferrocyanide pH 14 symmetric cell with SGL electrodes. Electrochemically cycled for 7 days, and then fully reduced to ferrocyanide; (c) 0.1 M potassium cyanide at pH 14; (d) 0.1 M ferrocyanide at pH 14, uncycled.

Figure 13. UV-Vis measured time-dependence of ferricyanide and total iron concentration in 3 mL of 0.5 mM ferricyanide pH 14 solution in contact and out of contact with 4 mm × 4 mm SGL electrode. Solutions were stored in glass vials.

Figure 14. (a) Potentiostatic cycling of 0.1 M ferri-/0.1 M ferrocyanide at pH 12, 13, and 14 in symmetric cells with HCBA electrodes; pH 12 and 13 are 5.8 mL CLS vs 11.0 mL NCLS, pH 14 is 5.7 mL CLS vs 11.0 mL NCLS. Cell data for pH 14 with SGL electrodes from Fig. 1 is included as comparison. (b) with zoomed in vertical scale.

Figure 6. Total decreased hydroxide concentration in the CLS of the symmetric cells from Figs. 1&5, measured after 5 days of cycling in a glovebox. ‘No electrode’ is a 0.1 M ferro/0.1 M ferricyanide solution at the given pH, identical to the starting CLS of each cell, left stirring in glovebox but without any contact with a carbon electrode.

Figure 15. Potentiostatic cycling of a 0.1 M ferri-/0.1 M ferrocyanide pH 14 symmetric cell (6 mL CLS vs 11 mL NCLS) with SGL electrodes. The NCLS was replaced after approximately 4 days, and 6 days, with 11 mL of fresh 50% SOC electrolyte. The CLS is discharged prior to NCLS replacement.

Figure 16. Potentiostatic cycling of a 0.1 M ferri-/0.1 M ferrocyanide pH 14 symmetric cell (6 mL vs 11 mL) with SGL electrodes. After 7 days of cycling (blue squares), the CLS was replaced with 6 mL of fresh 50% SOC electrolyte and cycled for 7 days (red circles). This CLS replacement was repeated a second time and again cycled for 7 days (black triangles).

Figure 17. Apparent capacity fade rates of potentiostatically cycled pH 14 symmetric cells with SGL electrodes and (a) 6 mL CLS vs 11 mL NCLS for various ferri-/ferrocyanide concentrations; (b) 0.1 M ferri-/0.1 M ferrocyanide, 12 mL CLS vs 22 mL NCLS, for various geometric surface areas of SGL electrodes per side. Lines are only meant to guide the eye.

Figure 18. Apparent capacity fade rates of potentiostatically cycled 0.1 M ferri-/0.1 M ferrocyanide pH 14 symmetric cells with SGL electrodes and (a) fixed NCLS volumes; (b) fixed 4 mL CLS volume. Lines are only meant to guide the eye.

Figure 11. Apparent capacity fade rates of potentiostatically cycled 0.1 M ferri-/0.1 M ferrocyanide pH 14 symmetric cells with SGL electrodes and fixed NCLS:CLS volume ratios. Lines are only meant to guide the eye.

References

[1]B.T. Huskinson, M.P. Marshak, C. Suh, S. Er, M.R. Gerhardt, C.J. Galvin, X. Chen, A. Aspuru-Guzik, R.G. Gordon, and M.J. Aziz, "A Metal-Free Organic-Inorganic Aqueous Flow Battery", *Nature* **505**, 195 (2014). https://doi.org/10.1038/nature12909

[2]K. Lin, Q. Chen, M.R. Gerhardt, L. Tong, S.B. Kim, L. Eisenach, A.W. Valle, D. Hardee, R.G. Gordon, M.J. Aziz, and M.P. Marshak, "Alkaline Quinone Flow Battery", *Science* **349**, 1529 (2015). https://doi.org/10.1126/science.aab3033

[3]T.B. Liu, X.L. Wei, Z.M. Nie, V. Sprenkle, and W. Wang, "A Total Organic Aqueous Redox Flow Battery Employing a Low Cost and Sustainable Methyl Viologen Anolyte and 4-HO-TEMPO Catholyte", *Advanced Energy Materials* **6**, 1501449 (2015). https://doi.org/10.1002/aenm.201501449

[4]T. Janoschka, N. Martin, M.D. Hager, and U.S. Schubert, "An Aqueous Redox-Flow Battery with High Capacity and Power: The TEMPTMA/MV System", *Angewandte Chemie International Edition* **55**, 14427 (2016). https://doi.org/10.1002/anie.201606472

[5]J. Luo, B. Hu, C. Debruler, and T.L. Liu, "A Pi-Conjugation Extended Viologen as a Two-Electron Storage Anolyte for Total Organic Aqueous Redox Flow Batteries", *Angewandte Chemie International Edition* **57**, 231 (2018). https://doi.org/10.1002/anie.201710517

[6]Z. Yang, L. Tong, D.P. Tabor, E.S. Beh, M.A. Goulet, D. De Porcellinis, A. Aspuru-Guzik, R.G. Gordon, and M.J. Aziz, "Alkaline Benzoquinone Aqueous Flow Battery for Large-Scale Storage of Electrical Energy", *Advanced Energy Materials* **8**, 1702056 (2018). https://doi.org/10.1002/aenm.201702056

[7]B. Hu, Y. Tang, J. Luo, G. Grove, Y. Guo, and T.L. Liu, "Improved Radical Stability of Viologen Anolytes in Aqueous Organic Redox Flow Batteries", *Chemical Communications* **54**, 6871 (2018). https://doi.org/10.1039/c8cc02336k

[8]D.G. Kwabi, K. Lin, Y. Ji, E.F. Kerr, M.-A. Goulet, D. De Porcellinis, D.P. Tabor, D.A. Pollack, A. Aspuru-Guzik, R.G. Gordon, and M.J. Aziz, "Alkaline Quinone Flow Battery with Long Lifetime at pH 12", *Joule* **2**, 1894 (2018). https://doi.org/10.1016/j.joule.2018.08.013

[9]Y.Y. Liu, S.F. Lu, S. Chen, H.N. Wang, J. Zhang, and Y. Xiang, "A Sustainable Redox Flow Battery with Alizarin-Based Aqueous Organic Electrolyte", *ACS Applied Energy Materials* **2**, 2469 (2019). https://doi.org/10.1021/acsaem.8b01512

[10]Y. Ji, M.A. Goulet, D.A. Pollack, D.G. Kwabi, S. Jin, D. Porcellinis, E.F. Kerr, R.G. Gordon, and M.J. Aziz, "A Phosphonate-Functionalized Quinone Redox Flow Battery at near-Neutral pH with Record Capacity Retention Rate", *Advanced Energy Materials* **9**, 1900039 (2019). https://doi.org/10.1002/aenm.201900039

[11]M.-A. Goulet, L. Tong, D.A. Pollack, D.P. Tabor, S.A. Odom, A. Aspuru-Guzik, E.E. Kwan, R.G. Gordon, and M.J. Aziz, "Extending the Lifetime of Organic Flow Batteries via Redox State Management", *Journal of the American Chemical Society* **141**, 8014 (2019). https://doi.org/10.1021/jacs.8b13295

[12]S. Jin, Y. Jing, D.G. Kwabi, Y. Ji, L. Tong, D. De Porcellinis, M.A. Goulet, D.A. Pollack, R.G. Gordon, and M.J. Aziz, "A Water-Miscible Quinone Flow Battery with High Volumetric Capacity and Energy Density", *ACS Energy Letters* **4**, 1342 (2019). https://doi.org/10.1021/acsenergylett.9b00739

[13]D.G. Kwabi, Y. Ji, and M.J. Aziz, "Electrolyte Lifetime in Aqueous Organic Redox Flow Batteries: A Critical Review", *Chemical Reviews* **120**, 6467 (2020). https://doi.org/10.1021/acs.chemrev.9b00599

[14]M. Wu, Y. Jing, A.A. Wong, E.M. Fell, S. Jin, Z. Tang, R.G. Gordon, and M.J. Aziz, "Extremely Stable Anthraquinone Negolytes Synthesized from Common Precursors", *Chem* **6**, 11 (2020). https://doi.org/10.1016/j.chempr.2020.03.021

[15] A. Hollas, X.L. Wei, V. Murugesan, Z.M. Nie, B. Li, D. Reed, J. Liu, V. Sprenkle, and W. Wang, "A Biomimetic High-Capacity Phenazine-Based Anolyte for Aqueous Organic Redox Flow Batteries", *Nature Energy* **3**, 508 (2018). https://doi.org/10.1038/s41560-018-0167-3

[16] R. Feng, X. Zhang, V. Murugesan, A. Hollas, Y. Chen, Y. Shao, E. Walter, N.P.N. Wellala, L. Yan, K.M. Rosso, and W. Wang, "Reversible Ketone Hydrogenation and Dehydrogenation for Aqueous Organic Redox Flow Batteries", *Science* **372**, 836 (2021). https://doi.org/10.1126/science.abd9795

[17] J. Xu, S. Pang, X. Wang, P. Wang, and Y. Ji, "Ultrastable Aqueous Phenazine Flow Batteries with High Capacity Operated at Elevated Temperatures", *Joule* ***5**, 2437* (2021). https://doi.org/10.1016/j.joule.2021.06.019

[18] G.B. Adams, R.P. Hollandsworth, and B.D. Webber, *Rechargeable Alkaline Zinc/Ferricyanide Battery: Final Report for the Period 29 September 1978-28 September 1979*. (Lockheed Palo Alto Research Laboratory, Lockheed Missiles & Space Co., Palo Alto, Calif., 1979).

[19] T. Janoschka, N. Martin, U. Martin, C. Friebe, S. Morgenstern, H. Hiller, M.D. Hager, and U.S. Schubert, "An Aqueous, Polymer-Based Redox-Flow Battery Using Non-Corrosive, Safe, and Low-Cost Materials", *Nature* **527**, 78 (2015). https://doi.org/10.1038/nature15746

[20] K. Wedege, E. Drazevic, D. Konya, and A. Bentien, "Organic Redox Species in Aqueous Flow Batteries: Redox Potentials, Chemical Stability and Solubility", *Scientific Reports* **6**, 39101 (2016). https://doi.org/10.1038/srep39101

[21] E.S. Beh, D. De Porcellinis, R.L. Gracia, K.T. Xia, R.G. Gordon, and M.J. Aziz, "A Neutral pH Aqueous Organic-Organometallic Redox Flow Battery with Extremely High Capacity Retention", *ACS Energy Letters* **2**, 639 (2017). https://doi.org/10.1021/acsenergylett.7b00019

[22] E. Drazevic, C. Szabo, D. Konya, T. Lund, K. Wedege, and A. Bentien, "Investigation of Tetramorpholinohydroquinone as a Potential Catholyte in a Flow Battery", *ACS Applied Energy Materials* **2**, 4745 (2019). https://doi.org/10.1021/acsaem.9b00351

[23] M. Park, E.S. Beh, E.M. Fell, Y. Jing, E.F. Kerr, D. De Porcellinis, M.A. Goulet, J. Ryu, A.A. Wong, R.G. Gordon, J. Cho, and M.J. Aziz, "A High Voltage Aqueous Zinc-Organic Hybrid Flow Battery", *Advanced Energy Materials* **9**, 1900694 (2019). https://doi.org/10.1002/aenm.201900694

[24] W. Ruan, J. Mao, S. Yang, and Q. Chen, "Communication—Tris(Bipyridyl)Iron Complexes for High-Voltage Aqueous Redox Flow Batteries", *Journal of The Electrochemical Society* **167**, 100543 (2020). https://doi.org/10.1149/1945-7111/ab9cc8

[25] X. Li, P. Gao, Y.-Y. Lai, J.D. Bazak, A. Hollas, H.-Y. Lin, V. Murugesan, S. Zhang, C.-F. Cheng, W.-Y. Tung, Y.-T. Lai, R. Feng, J. Wang, C.-L. Wang, W. Wang, and Y. Zhu, "Symmetry-Breaking Design of an Organic Iron Complex Catholyte for a Long Cyclability Aqueous Organic Redox Flow Battery", *Nature Energy* **6**, 873 (2021). https://doi.org/10.1038/s41560-021-00879-6

[26] Y. Jing, E.W. Zhao, M.-A.B. Goulet, Meisam , E.M. Fell, S. Jin, A. Davoodi, E. Jónsson, M. Wu, C.P. Grey, R.G. Gordon, and M.J. Aziz, "Electrochemical Regeneration of Anthraquinones for Lifetime Extension in Flow Batteries", *ChemRxiv* (2021). https://doi.org/10.33774/chemrxiv-2021-x05x1 (Accepted for publication in *Nature Chemistry*)

[27] J. Preusz, "Vermischte Chemische Notizen", *Annalen der Pharmacie* **29**, 323 (1839). https://doi.org/10.1002/jlac.18390290316

[28] S. Asperger, "Kinetics of the Decomposition of Potassium Ferrocyanide in Ultra-Violet Light", *Transactions of the Faraday Society* **48**, 617 (1952). https://doi.org/10.1039/tf9524800617

[29] C.A.P. Arellano and S.S. Martinez, "Effects of pH on the Degradation of Aqueous Ferricyanide by Photolysis and Photocatalysis under Solar Radiation", *Solar Energy Materials and Solar Cells* **94**, 327 (2010). https://doi.org/10.1016/j.solmat.2009.10.008

[30] M. Reinhard, T.J. Penfold, F.A. Lima, J. Rittmann, M.H. Rittmann-Frank, R. Abela, I. Tavernelli, U. Rothlisberger, C.J. Milne, and M. Chergui, "Photooxidation and Photoaquation of Iron

Hexacyanide in Aqueous Solution: A Picosecond X-Ray Absorption Study", *Structural Dynamics* **1**, 024901 (2014). https://doi.org/10.1063/1.4871751

[31] J. Luo, A. Sam, B. Hu, C. DeBruler, X. Wei, W. Wang, and T.L. Liu, "Unraveling pH Dependent Cycling Stability of Ferricyanide/Ferrocyanide in Redox Flow Batteries", *Nano Energy* **42**, 215 (2017). https://doi.org/10.1016/j.nanoen.2017.10.057

[32] M.-A. Goulet and M.J. Aziz, "Flow Battery Molecular Reactant Stability Determined by Symmetric Cell Cycling Methods", *Journal of The Electrochemical Society* **165**, A1466 (2018). https://doi.org/10.1149/2.0891807jes

[33] M. Cazot, G. Maranzana, J. Dillet, F. Beille, T. Godet-Bar, and S. Didierjean, "Symmetric-Cell Characterization of the Redox Flow Battery System: Application to the Detection of Degradations", *Electrochimica Acta* **321**, 134705 (2019). https://doi.org/10.1016/j.electacta.2019.134705

[34] T. Páez, A. Martínez-Cuezva, J. Palma, and E. Ventosa, "Revisiting the Cycling Stability of Ferrocyanide in Alkaline Media for Redox Flow Batteries", *Journal of Power Sources* **471**, 228453 (2020). https://doi.org/10.1016/j.jpowsour.2020.228453

[35] M. Hu, A.P. Wang, and T.L. Liu, "Cycling Performance and Mechanistic Insights of Ferricyanide Electrolytes in Alkaline Redox Flow Batteries", *ChemRxiv* (2022). https://doi.org/10.26434/chemrxiv-2022-lqms7-v2

[36] J.D. Benck, B.A. Pinaud, Y. Gorlin, and T.F. Jaramillo, "Substrate Selection for Fundamental Studies of Electrocatalysts and Photoelectrodes: Inert Potential Windows in Acidic, Neutral, and Basic Electrolyte", *PLoS ONE* **9**, e107942 (2014). https://doi.org/10.1371/journal.pone.0107942

[37] J. Luo, B. Hu, C. Debruler, Y.J. Bi, Y. Zhao, B. Yuan, M.W. Hu, W.D. Wu, and T.L. Liu, "Unprecedented Capacity and Stability of Ammonium Ferrocyanide Catholyte in pH Neutral Aqueous Redox Flow Batteries", *Joule* **3**, 149 (2019). https://doi.org/10.1016/j.joule.2018.10.010

[38] V.G. S, X. Zhang, F.C. MacNab, S. Kamal, D. Star, and G.W. Leach, "Scalable, Green Fabrication of Single-Crystal Noble Metal Films and Nanostructures for Low-Loss Nanotechnology Applications", *ACS Nano* **14**, 7581 (2020). https://doi.org/10.1021/acsnano.0c03466

[39] M. Bogdanov, R. Gryboś, and A. Samotus, "Electron-Transfer Kinetics and Mechanism of the Reduction of Octacyanometallates(IV) (M = Mo, W) by Hydroxide Ion in Aqueous Solution", *Transition Metal Chemistry* **18**, 599 (1993). https://doi.org/10.1007/BF00191133

[40] J. Feeney, A.S.V. Burgen, and E. Grell, "Cyanide Binding to Carbonic Anhydrase", *European Journal of Biochemistry* **34**, 107 (1973). https://doi.org/10.1111/j.1432-1033.1973.tb02735.x

[41] J. Seravalli and S.W. Ragsdale, "^{13}C NMR Characterization of an Exchange Reaction between CO and CO_2 Catalyzed by Carbon Monoxide Dehydrogenase", *Biochemistry* **47**, 6770 (2008). https://doi.org/10.1021/bi8004522

[42] T.M. Abbott, G.W. Buchanan, P. Kruus, and K.C. Lee, "^{13}C Nuclear Magnetic Resonance and Raman Investigations of Aqueous Carbon Dioxide Systems", *Canadian Journal of Chemistry* **60**, 1000 (1982). https://doi.org/10.1139/v82-149

[43] F. Mani, M. Peruzzini, and P. Stoppioni, "CO_2 Absorption by Aqueous NH_3 Solutions: Speciation of Ammonium Carbamate, Bicarbonate and Carbonate by a ^{13}C NMR Study", *Green Chemistry* **8**, 995 (2006). https://doi.org/10.1039/b602051h

[44] M. Shin, C. Noh, Y. Chung, and Y. Kwon, "All Iron Aqueous Redox Flow Batteries Using Organometallic Complexes Consisting of Iron and 3-[Bis (2-Hydroxyethyl)Amino]-2-Hydroxypropanesulfonic Acid Ligand and Ferrocyanide as Redox Couple", *Chemical Engineering Journal* **398**, 125631 (2020). https://doi.org/10.1016/j.cej.2020.125631

[45] C. Bleasdale, B.T. Golding, J. McGinnis, S. Müller, and W.P. Watson, "The Mechanism of Decomposition of *N*-Methyl-*N*-Nitrosourea in Aqueous Solution According to ^{13}C and ^{15}N NMR Studies:

Quantitative Fragmentation to Cyanate", *Journal of the Chemical Society, Chemical Communications* **24**, 1726 (1991). https://doi.org/10.1039/C39910001726

[46] J.S. Silvia and C.C. Cummins, "Two-Electron Reduction of a Vanadium(V) Nitride by CO to Release Cyanate and Open a Coordination Site", *Journal of the American Chemical Society* **131**, 446 (2009). https://doi.org/10.1021/ja807767w

[47] V.K. Krieble and J.G. McNally, "The Hydrolysis of Hydrogen Cyanide by Acids", *Journal of the American Chemical Society* **51**, 3368 (1929). https://doi.org/10.1021/ja01386a026

[48] V.K. Krieble and A.L. Peiker, "The Hydrolysis of Hydrogen Cyanide by Acids. II", *Journal of the American Chemical Society* **55**, 2326 (1933). https://doi.org/10.1021/ja01333a017

[49] J.D.F. Marsh and M.J. Martin, "The Hydrolysis and Polymerization of Hydrogen Cyanide in Alkaline Solutions", *Journal of Applied Chemistry* **7**, 205 (1957). https://doi.org/10.1002/jctb.5010070409

[50] E. Gail, S. Gos, R. Kulzer, J. Lorösch, A. Rubo, M. Sauer, R. Kellens, J. Reddy, N. Steier, and W. Hasenpusch, "Cyano Compounds, Inorganic," in *Ullmann's Encyclopedia of Industrial Chemistry* (2011). https://doi.org/10.1002/14356007.a08_159.pub3

[51] K.V. Greco, A. Forner-Cuenca, A. Mularczyk, J. Eller, and F.R. Brushett, "Elucidating the Nuanced Effects of Thermal Pretreatment on Carbon Paper Electrodes for Vanadium Redox Flow Batteries", *ACS Applied Materials & Interfaces* **10**, 44430 (2018). https://doi.org/10.1021/acsami.8b15793

[52] A. Forner-Cuenca, E.E. Penn, A.M. Oliveira, and F.R. Brushett, "Exploring the Role of Electrode Microstructure on the Performance of Non-Aqueous Redox Flow Batteries", *Journal of The Electrochemical Society* **166**, A2230 (2019). https://doi.org/10.1149/2.0611910jes

[53] A.A. Wong and M.J. Aziz, "Method for Comparing Porous Carbon Electrode Performance in Redox Flow Batteries", *Journal of The Electrochemical Society* **167**, 110542 (2020). https://doi.org/10.1149/1945-7111/aba54d

[54] D. Zhang, A. Forner-Cuenca, O.O. Taiwo, V. Yufit, F.R. Brushett, N.P. Brandon, S. Gu, and Q. Cai, "Understanding the Role of the Porous Electrode Microstructure in Redox Flow Battery Performance Using an Experimentally Validated 3D Pore-Scale Lattice Boltzmann Model", *Journal of Power Sources* **447**, 227249 (2020). https://doi.org/10.1016/j.jpowsour.2019.227249

[55] K.M. Tenny, A. Forner-Cuenca, Y.-M. Chiang, and F.R. Brushett, "Comparing Physical and Electrochemical Properties of Different Weave Patterns for Carbon Cloth Electrodes in Redox Flow Batteries", *Journal of Electrochemical Energy Conversion and Storage* **17**, 041010 (2020). https://doi.org/10.1115/1.4046661

[56] K.M. Tenny, K.V. Greco, M. van der Heijden, T. Pini, A. Mularczyk, A.-P. Vasile, J. Eller, A. Forner-Cuenca, Y.-M. Chiang, and F.R. Brushett, "A Comparative Study of Compressive Effects on the Morphology and Performance of Carbon Paper and Cloth Electrodes in Redox Flow Batteries", *Energy Technology* (2022). https://doi.org/10.1002/ente.202101162

[57] M.H. Chakrabarti, N.P. Brandon, S.A. Hajimolana, F. Tariq, V. Yufit, M.A. Hashim, M.A. Hussain, C.T.J. Low, and P.V. Aravind, "Application of Carbon Materials in Redox Flow Batteries", *Journal of Power Sources* **253**, 150 (2014). https://doi.org/10.1016/j.jpowsour.2013.12.038

[58] S. Dussi and C.H. Rycroft, "Less Can Be More: Insights on the Role of Electrode Microstructure in Redox Flow Batteries from Two-Dimensional Direct Numerical Simulations", *Physics of Fluids* **34**, 043111 (2022). https://doi.org/10.1063/5.0084066

[59] J. Luo, A.P. Wang, M. Hu, and T.L. Liu, "Materials Challenges of Aqueous Redox Flow Batteries", *MRS Energy & Sustainability* **9**, 1 (2022). https://doi.org/10.1557/s43581-022-00023-1

[60] Z. Yuan, Y. Duan, T. Liu, H. Zhang, and X. Li, "Toward a Low-Cost Alkaline Zinc-Iron Flow Battery with a Polybenzimidazole Custom Membrane for Stationary Energy Storage", *iScience* **3**, 40 (2018). https://doi.org/10.1016/j.isci.2018.04.006

[61] Y. Jing, M. Wu, A.A. Wong, E.M. Fell, S. Jin, D.A. Pollack, E.F. Kerr, R.G. Gordon, and M.J. Aziz, "*In Situ* Electrosynthesis of Anthraquinone Electrolytes in Aqueous Flow Batteries", *Green Chemistry* **22**, 6084 (2020). https://doi.org/10.1039/d0gc02236e

[62] T. Páez, A. Martínez-Cuezva, R. Marcilla, J. Palma, and E. Ventosa, "Mitigating Capacity Fading in Aqueous Organic Redox Flow Batteries through a Simple Electrochemical Charge Balancing Protocol", *Journal of Power Sources* **512**, 230516 (2021). https://doi.org/10.1016/j.jpowsour.2021.230516